Thermochimica Acta, 32 (1979) 277–291

THERMAL DECOMPOSITION OF BASIC MAGNESIUM CARBONATES UNDER HIGH-PRESSURE GAS ATMOSPHERES

YUTAKA SAWADA, JUNJI YAMAGUCHI, OSAMU SAKURAI, KEIZO UEMATSU, NOBUYASU MIZUTANI AND MASANORI KATO*

Department of Inorganic Materials, Faculty of Engineering, Tokyo Institute of Technology, O-okayama, Meguro-ku, Tokyo 152 (Japan)

(Received 16 October 1978)

ABSTRACT

Thermal decomposition of basic magnesium carbonates, hydromagnesite $4MgCO_3 \cdot Mg(OH)_2 \cdot 4H_2O$ and nesquehonite $MgCO_3 \cdot 3H_2O$, was studied under high-pressure carbon dioxide, nitrogen and argon atmospheres (≤ 50 kg cm^{-2}) by high-pressure DTA.

The decarbonation was strongly affected by the partial pressure of carbon dioxide. A new decomposition process with a new metastable intermediate was found at high-pressure carbon dioxide atmospheres: hydromagnesite, amorphous dehydrated, amorphous lower carbonate, intermediate, $MgCO_3$, MgO. A model was proposed to explain the decomposition mechanism integratedly throughout the various partial pressures of carbon dioxide; the formation of the intermediate governed the decarbonation rate and the crystallization of $MgCO_3$ from the amorphous lower carbonate at ~ 500 °C.

INTRODUCTION

Thermal decomposition of basic magnesium carbonates, hydromagnesite $4MgCO_3 \cdot Mg(OH)_2 \cdot 4H_2O$ and nesquehonite $MgCO_3 \cdot 3H_2O$, was highly dependent on the partial pressure of carbon dioxide (P_{CO_2})[1–7]. Two typical decarbonation processes for thermal decomposition of hydromagnesite found in the previous paper[8] are shown in Fig. 1:

type I (typical P_{CO_2}: ≤ 0.1 kg cm^{-2}). The dehydrated amorphous phase decomposed via the amorphous lower carbonate phase to MgO;

type II (typical P_{CO_2}: ~ 1.0 kg cm^{-2}). The dehydrated amorphous phase partially decarbonated (stage 1) to form the lower carbonate phase, then crystallization of $MgCO_3$ took place with an extremely sharp exothermic phenomenon and a rapid

* To whom correspondence should be addressed.

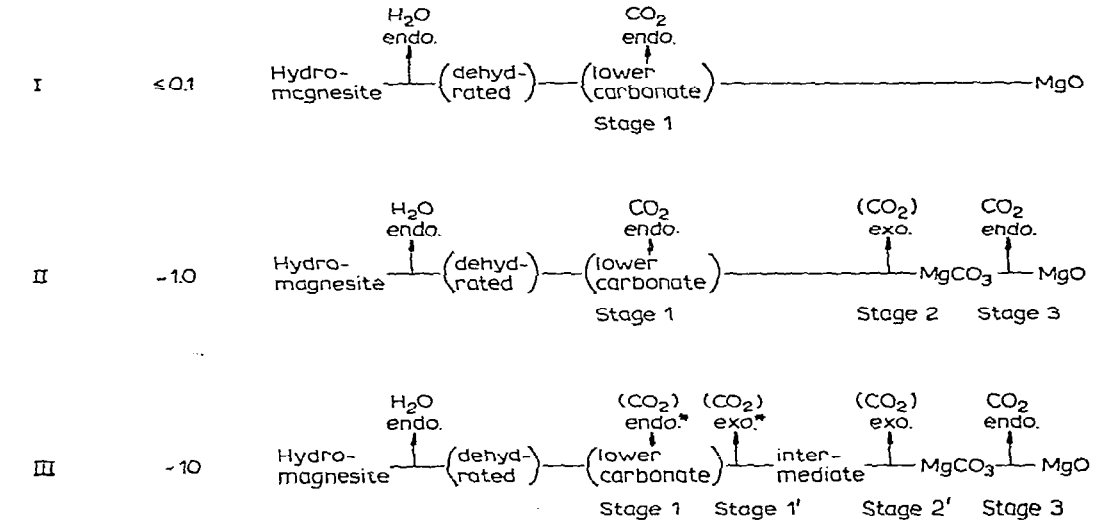

Fig. 1. Tentative diagram for thermal decomposition of hydromagnesite. Only the processes are shown in this diagram. The temperatures are not indicated. Endo = endothermic phenomenon; Exo = exothermic phenomenon; [] = amorphous phase; () = very small gas amount, * = not detected by DTA.

evolution of carbon dioxide at ~520°C (stage 2), and finally the $MgCO_3$ decomposed to MgO (stage 3).

However, the presence of two different decarbonation processes and the decrease of decarbonation rate at ~500°C (the end of stage 1 of type II) in carbon dioxide atmospheres were not fully explained. The phenomenon at ~520°C associated with $MgCO_3$ crystallization, a sharp exothermic peak in DTA and a rapid evolution of carbon dioxide should better be discussed further from a different view point.

In the present work the decomposition study was extended to higher pressures of carbon dioxide using high-pressure DTA ($P \leq 50$ kg cm^{-2}). The pressure dependence of the DTA peak temperatures was investigated for hydromagnesite and nesquehonite in carbon dioxide, nitrogen and argon atmospheres. A new decarbonation process (type III) was found. A new intermediate phase which was found by Suzuki and Ito[9] appeared during this process. The decomposition mechanisms at various partial pressures of carbon dioxide were discussed integratedly.

The so-called self-generated atmosphere is one of the greatest obstacles for decomposition study. When decarbonation in an inert gas atmosphere such as nitrogen, helium or argon, was studied, the carbon dioxide evolved from the specimen remained around the specimen without mixing with the surrounding inert gas atmospheres. This makes the actual partial pressure of carbon dioxide on the specimen much higher than that in the inert gas atmospheres supplied externally. When decarbonation is studied in vacuo, the actual partial pressure of carbon dioxide on the specimen surface might be higher than the pressure which was measured with some

pressure gauge located away from the specimen. It is impossible in both cases to measure the true partial pressure at a minute portion where the reaction occurs. The influence of the self-generated atmosphere can be offset or neglected in high-pressure carbon dioxide. This is an advantage of using high-pressure techniques for decomposition studies.

The difference between the equilibrium decomposition temperature and the peak temperature in DTA is a big problem. The peak in DTA reflects the temperature where the reaction rate is maximum. It is related only indirectly to the equilibrium decomposition temperature. The difference between these temperatures decreases with the increasing reaction rate. The reaction rate usually increases with the increasing temperature. The DTA peak temperature approaches the equilibrium decomposition temperature when the decomposition temperature is raised for a given decarbonation process by the increased partial pressure of carbon dioxide. Closer study of the decarbonation process is possible with high-pressure DTA. This is a significant advantage of the high-pressure decomposition study. High-pressure DTA was adopted for the thermal decomposition of basic magnesium carbonates.

EXPERIMENTAL

Specimens

Hydromagnesite. Magnesium hydroxide carbonate G. R. (Merck, West Germany) was used. The $MgO:CO_2:H_2O$ ratio (1.00:0.80:1.12) determined by the compositional analysis was only slightly different from that of the pure hydromagnesite $4MgCO_3 \cdot Mg(OH)_2 \cdot 4H_2O$ (1.00:0.80:1.00). The ratio was closer to that of the ideal composition than that of Wako Pure Chemical Industries Ltd., Japan (1.00:0.75:0.96) which was used in the previous work[7, 8]. X-ray powder

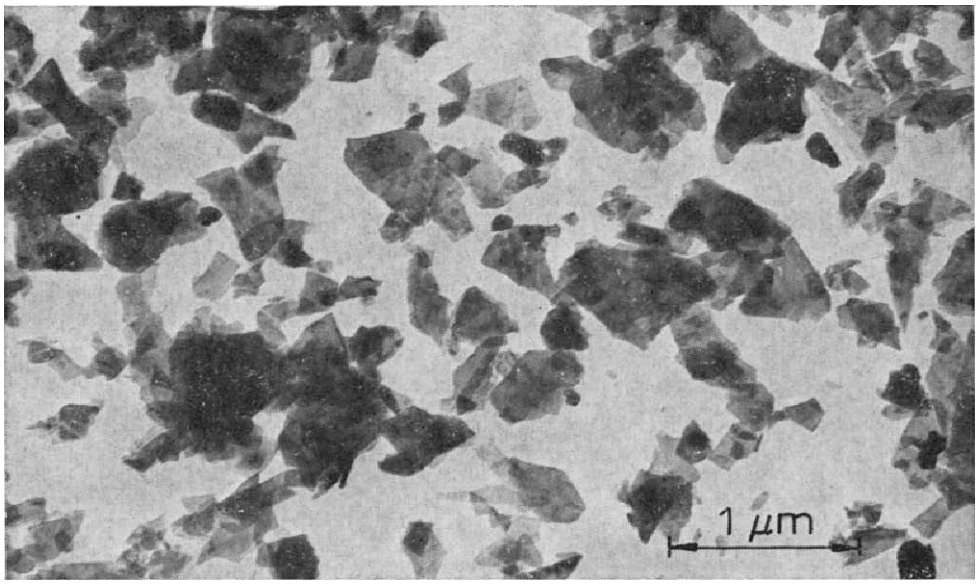

Fig. 2. Electron micrograph of hydromagnesite.

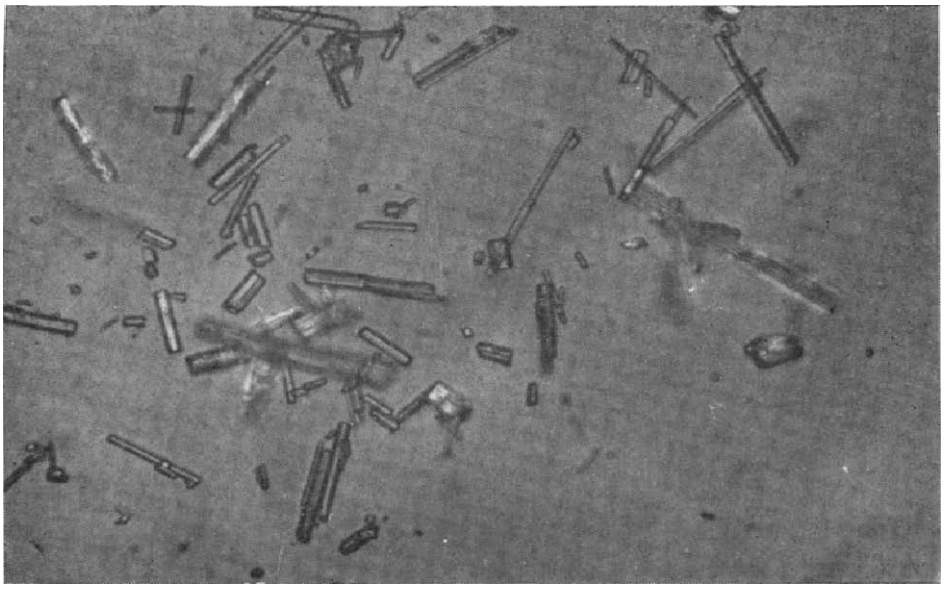

Fig. 3. Optical micrograph of nesquehonite.

diffraction of the present specimen showed the pattern of hydromagnesite[10] more clearly than the previous specimen. The electron micrograph of the specimen is shown in Fig. 2. The specimen was a platelet of ~0.1–1.0 μm in length and ~0.05 μm in thickness. Electron diffraction revealed that each particle was polycrystalline.

Nesquehonite. Nesquehonite was synthesized from $MgCl_2 \cdot 6H_2O$ and Na_2CO_3 (special reagent grade, Wako Pure Chemical Industries Ltd., Japan) by a method similar to that of Doi and Kato[4]. $MgCl_2 \cdot 6H_2O$ (1 M aq.) and Na_2CO_3 (1 M aq.) was mixed slowly at 0°C. The resultant white precipitate was filtered, washed with distilled water and dissolved in water saturated with carbon dioxide. After further filtration, the water was kept at 5°C for 24 h and at 20°C for 48 h. White fine crystals were precipitated on the walls. They were removed with a spatula, filtered, washed with distilled water and dried in a flow of carbon dioxide at 20°C for 48 h. The $MgO:CO_2:H_2O$ ratio (1.00:1.02:3.14) was very close to the stoichiometric composition of nesquehonite $MgCO_3 \cdot 3H_2O$ (1.00:1.00:3.00). Optical microscopic observation (Fig. 3) showed that the specimen consisted of needle-like single crystals of ~5–20 μm in length and ~1–3 μm in diameter. Powder X-ray diffraction showed extremely sharp peaks of nesquehonite[11]. No peak of hydromagnesite was observed.

High-pressure DTA

Construction of the high-pressure DTA equipment is shown in Fig. 4A and B. The apparatus was designed and made by the authors. The specimen was heated in a flow of high-pressure carbon dioxide, nitrogen or argon atmosphere ($P \leq 50$ kg cm^{-2}) at ~10°C min^{-1} up to 700°C. The atmosphere in the specimen chamber was changed by filling (~5 kg cm^{-2}) and letting out the gas three times before the experiment.

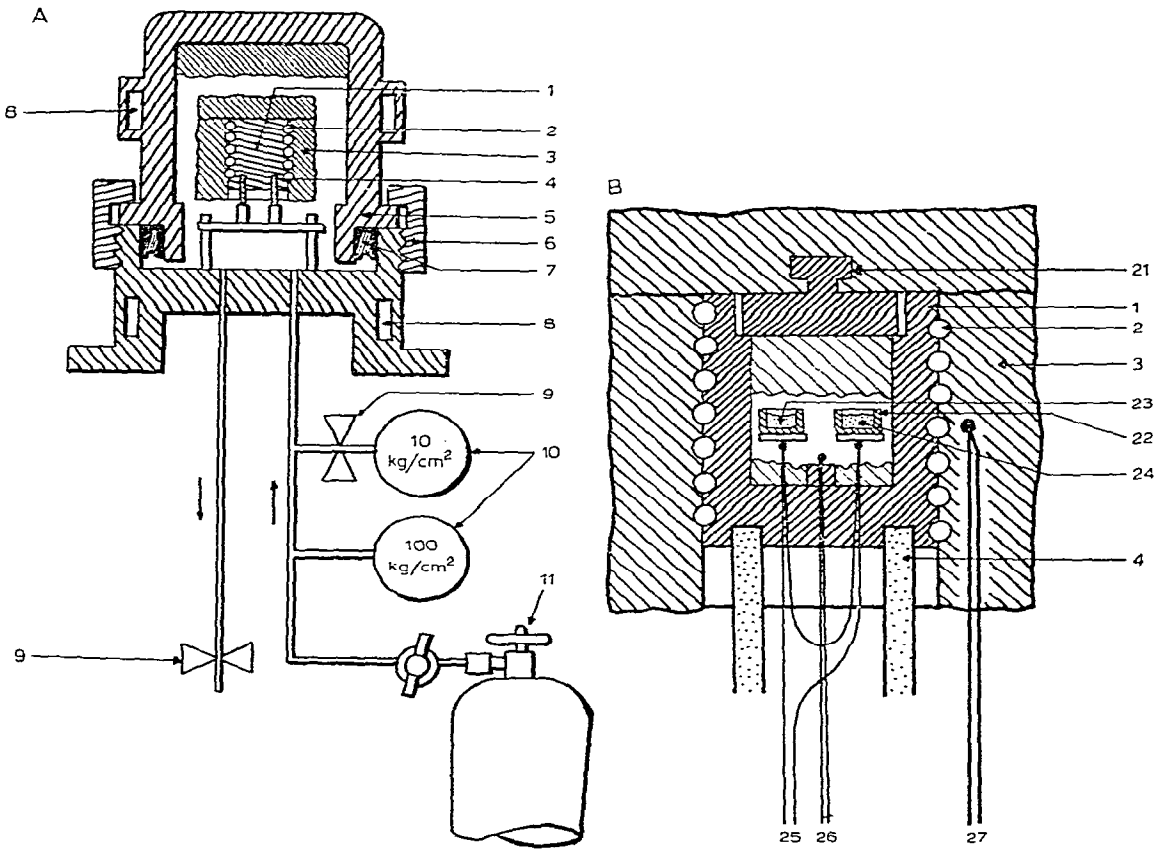

Fig. 4A. Construction of high-pressure DTA apparatus. 1, Nickel block in which the DTA measuring cell is installed as shown in Fig. 4B; 2, a sheated heater (1.5 mmø); 3, mulite wool; 4, alumina pipe; 5, high-pressure vessel (100 mm outer diameter) made of steel; 6, screw for fixing the high-pressure vessel 5; 7, a U-shaped packing ring made of rubber; 8, cooling water tubes; 9, valves; 10, pressure gauges (10 kg cm^{-2} and/or 100 kg cm^{-2}, $\pm$ 1.5%); 11, gas cylinder (CO_2, N_2 or Ar). B. Construction of measuring cell of the high-pressure DTA. 1, Nickel block (25 mm outer diameter); 2, sheathed heater (1.5ø); 3, mulite wool; 4, alumina pipe; 21, nickel cap; 22, DTA specimen container (5 mmø × 2.5 mm, platinum, 115 mg); 23, specimen (hydromagnesite: 8 mg, nesquehonite: 15 mg); 24, standard (alumina: 8 mg); 25, thermocouple for DTA measurement (Pt–Pt/Rh13%), DTA recorder range: 100 or 200 μV; 26, thermocouple for temperature measurement (Pt–Pt/Rh13%), no cold junction was used, referenced to room temperature; 27, thermocouple for temperature control (Pt–Pt/Rh13%).

Compositional analysis

Carbon contents in the decomposed specimens were measured with a C-elementary analysis apparatus. The specimen (~2–5 mg) was heated at ~850°C for 5 min in a helium–oxygen mixture (mixing ratio 9:1) and the amount of carbon dioxide was quantitatively measured by gas chromatography.

Powder X-ray diffraction analysis

The structural changes of the quenched specimens were measured by a powder X-ray diffractometer (Philips Co., target: Cu, filter: Ni, scan speed: 2θ = 2.0°C min^{-1}). For the precise measurement of the newly found intermediate, the scan speed of

$2\theta = 0.25°\ min^{-1}$ was used. The angle was calibrated with NBS standard silicon and ground natural hydromagnesite from Soghan, Iran. This material showed sharp diffraction peaks and improved the precision at low angles. The powder diffraction diagram for the intermediate was successfully indexed with a Wang 600-14 minicomputer (1848 steps/247 words, Wang Laboratories, Inc., U.S.A.). The program of Sawada et al.[12] was used. Cubic, tetragonal and hexagonal systems were examined. Graphical hand indexing was also attempted using Frevel's charts[13–15] and Battle indexing charts[16].

IR spectrum analysis

The IR spectrograph was recorded at room temperature (IR-G, Japan Spectroscopic Co., Japan). Approximately 0.1 mg of the specimen was mixed with ~200 mg KBr and pressed into a pellet. Natural magnesite from Korea was used as a reference.

Synthesis of the intermediate

Hydromagnesite powder was heated at $P_{CO_2} = 0.5$ kg cm^{-2} (mixture of helium and carbon dioxide) at ~10°C min^{-1} to 350°C and quenched to room temperature. The specimen (~40 mg) was placed in a silver tube (3 mmø × 50 mm) with one end open and inserted into a pressure vessel for hydrothermal synthesis (Nikkiso Co., Ltd., Japan). It was heated at ~10°C min^{-1} to ~500°C at $P_{CO_2} =$ 6.0 kg cm^{-2} under nominally dry conditions. After quenching to room temperature by blasting air externally, the tube was removed.

RESULTS

High-pressure DTA

An example of high-pressure DTA for thermal decomposition of hydromagnesite in carbon dioxide ($P_{CO_2} = 21$ kg cm^{-2}) is shown in Fig. 5A. Dehydration (endothermic reaction) took place at ~200–300°C. A sharp exothermic phenomenon (stage 2) was observed at ~485°C. Decarbonation (stage 2, endothermic reaction) took place at ~630–680°C. The DTA peak profiles were basically the same throughout the present experiments. Decarbonation stage 1 found in type II (endothermic reaction) was absent. The peak temperatures changed with the ambient pressure. Similar DTA results were obtained for nesquehonite. Decarbonation stage 1 (endothermic reaction) which was detected in the previous study at $P_{CO_2} \leq 1$ kg cm^{-2} was not found at $P_{CO_2} = 0$ kg cm^{-2} by the present instrument. The sensitivity of the high-pressure DTA is probably lower than that of the previous instrument.

Thermal decomposition of hydromagnesite at $P_{CO_2} = 21$ kg cm^{-2}

Thermal decomposition of hydromagnesite under a high-pressure carbon dioxide atmosphere was investigated in more detail; a new decomposition process was found, which the authors will hereafter call "type III' (typical $P_{CO_2} = 10$ kg cm^{-2}). The tentative diagram for type III is shown in Fig. 1.

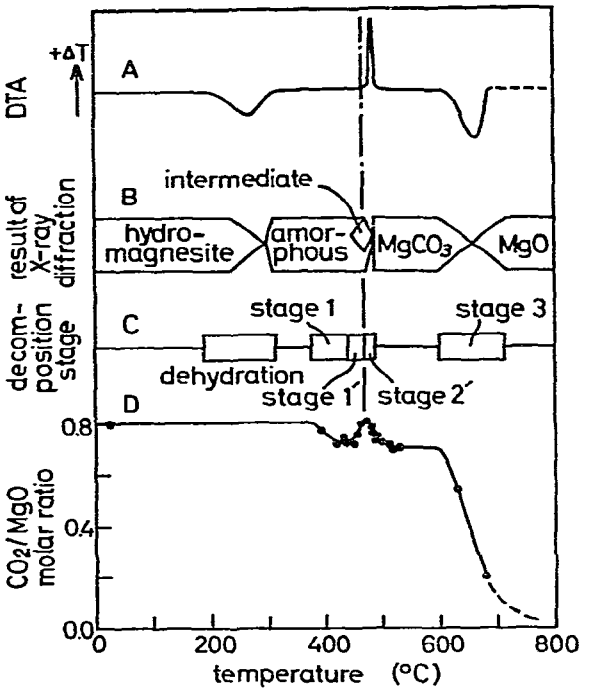

Fig. 5. Thermal decomposition of hydromagnesite at P_{CO_2} = 21 kg cm^{-2}. Specimen weight, 8 mg; heating rate, 10°C min^{-1}. A, High-pressure DTA; B, results of X-ray diffraction analysis for the specimens quenched from the various temperatures; C, decomposition stages; D, CO_2/MgO molar ratio for the quenched specimen.

High-pressure DTA for thermal decomposition of hydromagnesite in carbon dioxide (P_{CO_2} = 21 kg cm^{-2}) is shown in Fig. 5A. The predominant phases in the specimens quenched from various temperatures are shown in Fig. 5B. The width of the band in the figure represents schematically the amount of phase in the specimen. The decomposition stages are shown in Fig. 5C. The CO_2/MgO molar ratios of the quenched specimens are shown in Fig. 5D.

The specimen showed an X-ray diffraction pattern of hydromagnesite up to ~300°C where the dehydration proceeded. An amorphous diffraction pattern was observed up to 400°C. Slight decarbonation was observed at 350–400°C (stage 1) by compositional analysis. The corresponding endothermic peak was not detected in the present study. The extent of the decarbonation was probably below the detection limit of the high-pressure DTA.

The increase in CO_2/MgO molar ratios was found at 450–490°C; maximum at ~470°C. X-ray diffraction showed a new intermediate pattern which will be discussed later. The diffraction peak intensities were correlated with the CO_2/MgO molar ratios. Thus a small amount of carbon dioxide was incorporated into the amorphous lower carbonate phase to form the intermediate at 450–490°C. The authors will hereafter call this process "stage 1". No exothermic peak corresponding to the carbonation was found, probably due to the present detection limit.

$MgCO_3$ crystallized suddenly (X-ray diffraction) with a sharp exothermic

phenomenon (high-pressure DTA). Rapid evolution of carbon dioxide took place simultaneously with the crystallization of $MgCO_3$ and the sharp exothermic phenomenon. It should be noted that $MgCO_3$ crystallized slightly after passing the maximum formation of the intermediate. No change was found in DTA during the decarbonation process immediately before crystallization. The heat of this decarbonation phenomenon was probably small and compensated by the simultaneous strong exothermic phenomenon. These are called "stage 2'". Stage 2' is similar to stage 2 in type II. The precise mechanism of stage 2' in type III may not be the same as stage 2 in type II; the decrease of the intermediate was included.

At the higher temperature, decomposition of $MgCO_3$ began (stage 3, 630–680°C). The X-ray diffraction peak intensities of $MgCO_3$ were proportional to the CO_2/MgO molar ratios. The X-ray diffraction pattern of MgO was found in the specimen when the decarbonation was almost complete.

The effect of pressures on high-pressure DTA peak temperatures

Figure 6 shows the effect of pressure on the high-pressure DTA peak temperatures during the thermal decomposition of hydromagnesite and nesquehonite in various gases (carbon dioxide, nitrogen and argon). Since the dehydration temperature (~200–300°C) was not affected by the pressures, it was omitted in the figure.

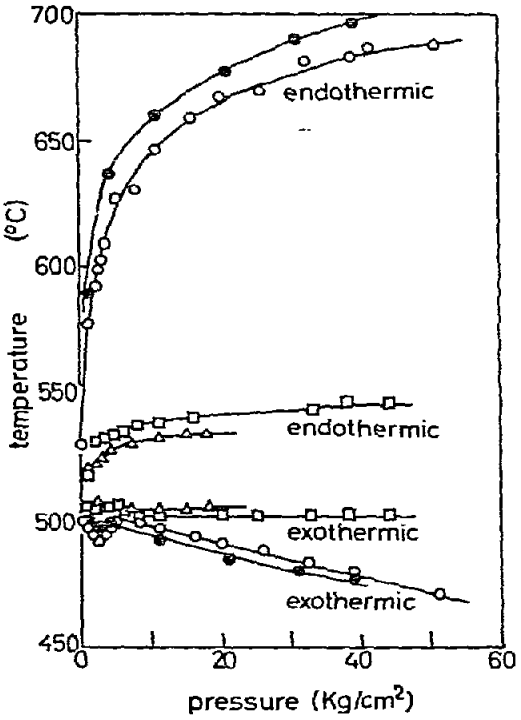

Fig. 6. The effect of pressure on high-pressure DTA peak temperatures for thermal decomposition of hydromagnesite and nesquehonite in various gases (CO_2, N_2 and Ar). Hydromagnesite (8 mg) in ○, CO_2; □, N_2; △, Ar. ●, Nesquehonite in CO_2. Heating rate: 10°C min^{-1}. The peak at 200–300°C due to dehydration (endothermic reaction) has been omitted.

The decarbonation temperature was affected remarkably by the partial pressure of carbon dioxide. The peak temperature for stage 2′ (exothermic phenomenon) changed approximately linearly with P_{CO_2}. As P_{CO_2} increased from ~1 to 50 kg cm^{-2}, the peak temperature of stage 2′ decreased by ~30°C. A small valley was observed at P_{CO_2} = ~3 kg cm^{-2}. A similar change was found for nesquehonite. At $P_{CO_2} \leq 1$ kg cm^{-2}, the decarbonation peak temperature in stage 2′ for hydromagnesite was ~20°C lower than that of the previous study[7, 8]. This should be attributed to the difference in the specimens and the instruments. The decarbonation temperature of stage 2′ (504°C) was not affected by the pressure of nitrogen and argon when the pressure exceeded 10 kg cm^{-2}. A minute deviation from this behavior was observed at P_{N_2} or $P_{Ar} \leq 5$ kg cm^{-2}.

The peak temperature of stage 3 (endothermic reaction) increased with P_{CO_2} in both hydromagnesite and nesquehonite; the peak temperature changed markedly at $P_{CO_2} \leq$ ~1 kg cm^{-2} but saturated gradually at higher P_{CO_2}. A slight difference (~10–20°C) was found, however, between the peak temperatures in hydromagnesite and nesquehonite for stage 3 in carbon dioxide atmospheres.

In stage 3 under high pressures of nitrogen and argon, the peak temperature in hydromagnesite increased markedly with pressure at ≤10 kg cm^{-2} and gradually saturated, as with that found in carbon dioxide atmospheres. However, the peak temperatures (~520–550°C) in high-pressure nitrogen and argon atmospheres were much lower than in carbon dioxide atmospheres (~600–700°C).

High-pressure DTA peak half-widths for decarbonation stage 3 of nesquehonite at various carbon dioxide pressures are shown in Fig. 7. The half-widths decreased with increasing P_{CO_2}. This results suggest that the decomposition rate increased at high P_{CO_2}. This behavior can be understood by the increased reaction rate at high temperature; the increased P_{CO_2} raised the decomposition temperature. The half-widths for decarbonation of hydromagnesite were approximately constant with P_{CO_2}. The peak

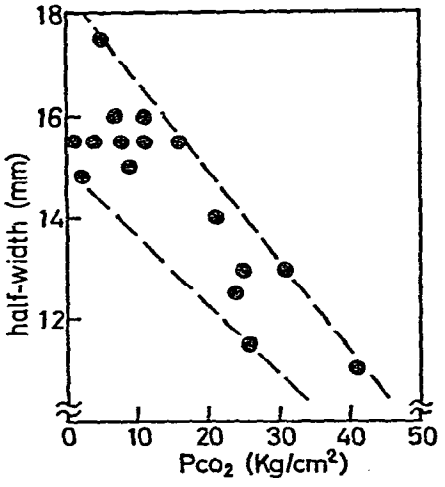

Fig. 7. High-pressure DTA peak half-widths for decarbonation stage 3 of nesquehonite at various carbon dioxide pressures. Specimen weight, 15 mg; heating rate, 10°C min^{-1}.

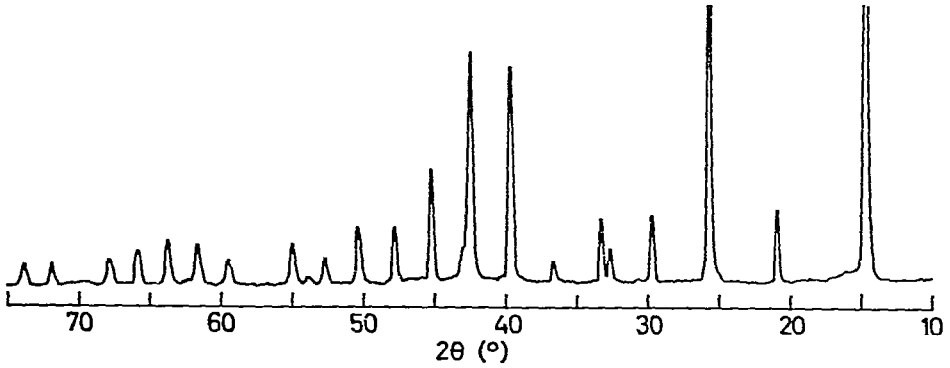

Fig. 8. Powder X-ray diffraction pattern of the intermediate.

TABLE 1

POWDER X-RAY DIFFRACTION DATA OF THE INTERMEDIATE

Observed peaks			*Possible system/lattice constants (Å) and indices*	
No.	*d (Å)*	*I/I₀*	*Cubic* $a = 8.5193 \pm 0.0049$	*Hexagonal* $a = 6.9527 \pm 0.0005$, $c = 4.2580 \pm 0.0005$
1	6.0268	100	110	100
2	4.2538	7	200	001
3	3.4788	44	211	101 110
4	3.0127	7	220	200
5	2.6957	7	310	111
6	2.4613	2	222	201
7	2.2775	26	321	210
8	2.1313	35	400	002
9	2.0091	16	411 330	102 211 300
10	1.9063	8	420	(No indices)
11	1.8170	8	332	112 301
12	1.7396	3	422	202 220
13	1.6708	6	510 431	310
14	1.5554	4	521	212 311
15	1.5054	6	440	400
16	1.4604	7	530 433	302
17	1.4191	6	600 442	003 401
18	1.3814	4	611 532	103 320
19	1.3137	3	541	113 312 321 410
20	1.2839	3	622	203
21	1.2042	2	710 550 543	213 500
22	0.9897	3	831 750 743	323 430

heights and widths of the exothermic peaks were approximately constant for both compounds.

The intermediate

The new intermediate phase found in high-pressure carbon dioxide atmospheres was examined in detail.

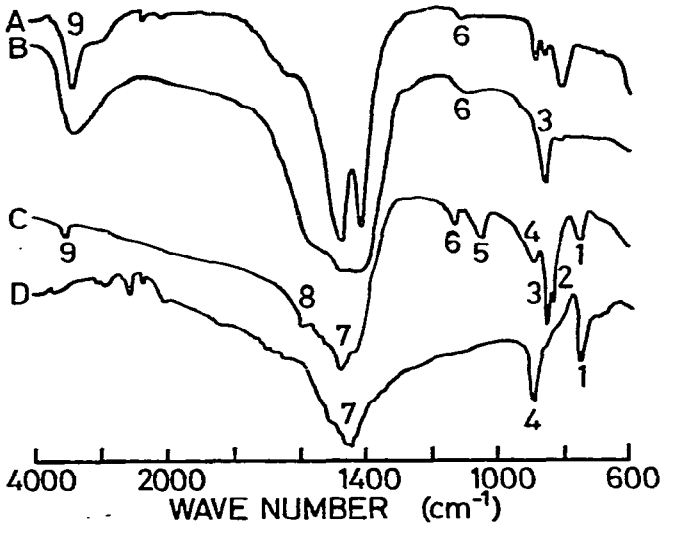

Fig. 9. IR spectra for the intermediate, etc. A, Hydromagnesite; B, the amorphous phase ("lower carbonate"); C, the intermediate; D, natural $MgCO_3$ from Korea.

Powder X-ray diffraction. The powder X-ray diffraction pattern of the intermediate is shown in Fig. 8. The diffraction was sharp and strong. The analysis of diffraction peaks are presented in Table 1. A peak (d = 2.7570 Å, v/I_0 = 4) was excluded from Table 1 since it was identified as the strongest $MgCO_3$ diffraction (104) which was supposed to co-exist. The peaks (Nos. 1–19) were the same as those found by Suzuki and Ito[9] when they heated natural nesquehonite in air. The powder diffraction data were successfully indexed as shown in Table 1; all 22 peaks were indexed by the cubic system and/or all peaks except No. 10 were indexed by the hexagonal system.

IR spectrum. The IR spectrum of the intermediate is shown in Fig. 9C. IR spectra of hydromagnesite, the amorphous phase which the authors called "lower carbonate" in the previous paper[8] and natural $MgCO_3$ from Korea are shown in Fig. 9A, B and D, respectively, for reference.

The absorption bands Nos. 2 (833 cm^{-1}), 3 (843 cm^{-1}) and 4 (882 cm^{-1}) were all assigned to CO_3^{2-} bending vibrations[17–19]. The sharp and strong absorption band No. 2 was assigned to the intermediate. The sharp and strong absorption band No. 3 was obviously assigned to the intermediate though it was close to the absorption band of the lower carbonate (850 cm^{-1}). The broad absorption band No. 5 (1040 cm^{-1}) was assigned to the intermediate; its vibration mode was not characterized. The broad absorption band No. 6 (1125 cm^{-1}) was close to CO_3^{2-} ν_1 symmetric stretching vibration[20]. The strong absorption range No. 7 (1400–1700 cm^{-1}) was due to CO_3^{2-} ν_3 asymmetric stretching vibration[17–20]. The weak absorption band No. 8 (~1580 cm^{-1}) was assigned to the intermediate.

The absorption bands at 3000–3500 cm^{-1} due to H_2O or OH vibration were very weak and broad, suggesting that the intermediate contains neither H_2O nor OH in the structure but only absorbed water.

TABLE 2

ANALYTICAL RESULTS FOR THE QUENCHED SPECIMENS WHICH SHOWED POWDER X-RAY DIFFRACTION OF THE INTERMEDIATE

Specimen	*Molar ratios*		*Specimen preparation (syntheses)*[a]		
	CO_2/MgO	CO_2/MgO	*Apparatus*[b]	P_{CO_2} ($kg\ cm^{-2}$)	*Quenching temperatures* (°C)
A	0.69	0.26	1	6	500
	0.72	0.25			
B	0.82	0.17	2	6	514
	0.84	0.20			486
C	0.81	0.13	2	20	465
	0.79	0.08			480
	0.75	0.10			487
D	0.83	0.20	2	35	452
	0.81	0.13			462
	0.74	0.11			471
	0.80	0.10			489
	0.78	0.10			485

[a] Heated in high-pressure carbon dioxide at 10 °C min^{-1} and quenched to room temperature.
[b] 1 = Nikkiso hydrothermal tube; cooled at the high pressure. 2 = High pressure DTA; cooled after evacuation of the high pressure gas.

Basic magnesium carbonate, hydromagnesite, nesquehonite and artinite $MgCO_3 \cdot Mg(OH)_2 \cdot 3H_2O$ were not found. They have strong and sharp absorption bands due to H_2O or OH vibration. The absorption bands due to CO_3^{2-} vibrations were not consistent.

The intermediate specimen contained a small amount of $MgCO_3$. It is probable that some $MgCO_3$ absorption bands are superimposed on the absorption bands of the intermediate. The absorption bands Nos. 1 (742 cm^{-1}), 4 (882 cm^{-1}) and 7 (1400–1600 cm^{-1}) were assigned to $MgCO_3$ spectrum. The absorption band No. 1 was assigned to ν_4 planar bending vibration of CO_3^{2-}. The absorption band No. 4 was assigned to ν_2 out-of-plane bending vibration (880 cm^{-1}). The absorption band No. 7 was assigned to the CO_3^{2-} ν_3 asymmetric stretching vibration.

Careful attention should also be paid to some other compounds co-existing in the intermediate except $MgCO_3$ and the lower carbonate.

Composition. Table 2 shows the results of compositional analysis on the quenched specimens which showed the intermediate phase in the powder X-ray diffraction. The composition determination was only partially successful. The results varied in different runs.

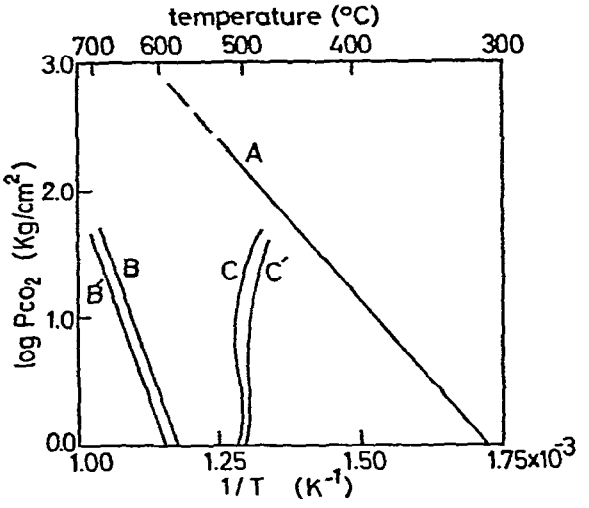

Fig. 10. The equilibrium relation between $MgCO_3 \rightleftarrows MgO + CO_2$ and log P_{CO_2} vs. the reciprocal of the absolute temperature of the high-pressure DTA peak of stage 3 for hydromagnesite and nesquehonite. A, The equilibrium relation between $MgCO_3 \rightleftarrows MgO + CO_2$ calculated with the reported thermodynamic data[21]; B, high-pressure DTA peak of stage 3 for hydromagnesite; B′, high pressure DTA peak of stage 3 for nesquehonite; C, high pressure DTA peak of the stage 2′ for hydromagnesite; C′, high pressure DTA peak of the stage 2′ for hydromagnesite.

DISCUSSION

The equilibrium P_{CO_2} for the reaction[21]

$$MgCO_3 \rightleftarrows MgO + CO_2$$

is shown in Fig. 10A. Log P_{CO_2} was plotted against the reciprocal absolute peak temperatures of high-pressure DTA for hydromagnesite and nesquehonite in Fig. 10B, B′, C and C′. The dehydration peaks were excluded. These peaks appeared in the region where MgO is more thermodynamically stable than $MgCO_3$. Both the intermediate and $MgCO_3$ are essentially metastable in this region.

The predominant effects of P_{CO_2} and CO_2/MgO molar ratio in the specimen on the decomposition process were described in the previous paper[18] and confirmed in the present study.

The intermediate had higher CO_2/MgO molar ration than that of the lower carbonate (Fig. 5D). The formation of the intermediate was favored at high P_{CO_2}. The intermediate was apparently stable within a limited temperature range, 450–470 °C at $P_{CO_2} = 21$ kg cm^{-2}. It probably has a cubic or hexagonal structure. The CO_2/MgO molar ratio of the amorphous lower carbonate was also expected to increase with increasing P_{CO_2}. In the previous study, the sharp exothermic peak in DTA was explained by the heat of crystallization. This study shows two phases before the crystallization process, amorphous lower carbonate and intermediate. Definite assignment of the phase from which $MgCO_3$ crystallized is not attempted. However, the amorphous lower carbonate is probably responsible for the exothermic phenomenon. The heat of crystallization from the amorphous phase is, as expected, higher

than that of the phase transition within crystalline phases. After the intermediate decreased slightly (stage 2'), the amorphous lower carbonate suddenly crystallized to $MgCO_3$ with a sharp exothermic phenomenon. The heat of crystallization raised the actual specimen temperature and accelerated the decomposition rate of the intermediate. The evolution of carbon dioxide in type III was different to that in type II. The decomposition of $MgCO_3$ was not included in type III. Crystallized $MgCO_3$ did not decompose in type III until 600–700 °C under high P_{CO_2} conditions.

The decarbonation rate decreased with increasing temperature in type II stage 1 as reported in the previous paper[7, 8]. This result can be understood by assuming the competition between the reactions of the intermediate formation and the lower carbonate formation. Provided the intermediate was rather stable compared to the lower carbonate, the overall decarbonation rate decreases if the reaction rate of the intermediate formation relative to the lower carbonate formation increased with increasing temperature.

The peak temperature of stage 3 changed significantly at $P_{CO_2} \leq 1$ kg cm^{-2} and saturated at higher P_{CO_2} as shown in Fig. 6. This tendency can be explained qualitatively by assuming the mass action law for the reaction

$$MgCO_3 \rightleftarrows MgO + CO_2$$

Approximately linear relations were observed between the reciprocal DTA peak temperature and the logarithm of P_{CO_2} (Fig. 10B and B'). However, this is far from the quantitative understanding. The ΔH and ΔS for the decomposition processes of hydromagnesite and nesquehonite were calculated by least squares method; ΔH = 50.85 and 57.14 kcal mole^{-1} and ΔS = 60.13 and 66.26 cal mole^{-1} K, respectively. The enthalpy and entropy for the actual decarbonation processes deviated markedly from the equilibrium between $MgCO_3$ and MgO (ΔH = 24.03 kcal mole^{-1} and ΔS = 41.15 cal mole^{-1} K[21]). These large deviations show the existence of various factors influencing the apparent decarbonation temperature. These differences were expected since the thermodynamic decomposition temperature and the apparent decarbonation temperature in DTA were not directly related. The apparent decarbonation temperature in DTA represents the temperature at which the decarbonation rate was maximum under a constant heating rate. It is a complicated variable affected by many factors; heating rate, heat transfer, and, most important, the rate of solid state reaction. With the increasing temperature, the reaction rate generally increases and the influence of the reaction rate on the apparent decomposition temperature becomes less important. At higher temperatures, the apparent decarbonation temperature is expected to approach the equilibrium decomposition temperature. This was found in Fig. 10; the deviation from the equilibrium decreased as the partial pressure of carbon dioxide (or temperature) increased. This was found in Fig. 6; decomposition was completed in a shorter period as the temperature increased. At lower temperature, the reaction rate was extremely low. This explains the absence of a reverse reaction, formation of $MgCO_3$ from MgO, under low P_{CO_2}.

The peak temperature of DTA in decarbonation stage 3 under high-pressure

nitrogen or argon (Fig. 6) increased at $P \lesssim 10$ kg cm^{-2} and saturated at the higher pressure. The behavior is similar to that found in the carbon dioxide atmosphere. However, the peak temperatures (520–550 °C) were much lower than those in the carbon dioxide atmosphere (600–700 °C). This can be explained by the presence of a self-generated atmosphere of carbon dioxide; carbon dioxide evolved from the specimen remained around the specimen surface. The true P_{CO_2} around the specimen was considerably higher during the decomposition process. The decarbonation temperatures of stage 3 in a nitrogen or argon atmosphere was ~520–550 °C. This corresponded to the decarbonation in carbon dioxide atmospheres of $P_{CO_2} = \sim 1$–2 kg cm^{-2}. The actual P_{CO_2} around the specimen was estimated to be ~1–2 kg cm^{-2}. The effect of the self-generated atmosphere can be neglected at $P_{CO_2} > 1$–2 kg cm^{-2}.

ACKNOWLEDGEMENT

The authors thank Mr. T. Saito of the Laboratory of Resources Utilization of the Tokyo Institute of Technology for the compositional analysis.

REFERENCES

1 R. M. Dell and S. W. Weller, *Trans. Faraday Soc.*, 55 (1959) 2203.
2 H. Hashimoto, T. Tomizawa and M. Mitomo, *Kogyo Kagaku Zasshi*, 71 (1968) 480.
3 N. Morandi, *Mineral. Petrogr. Acta*, 15 (1969) 93.
4 A. Doi and C. Kato, *Kogyo Kagaku Zasshi*, 74 (1971) 1597.
5 W. Höland and K. Heide, *Thermochim. Acta*, 15 (1976) 287.
6 T. Tomizawa, S. Hara and H. Hashimoto, *Yogyo Kyokai Shi*, 84 (1976) 259.
7 Y. Sawada, K. Uematsu, N. Mizutani and M. Kato, *J. Inorg. Nucl. Chem.*, 40 (1978) 979.
8 Y. Sawada, K. Uematsu, N. Mizutani and M. Kato, *Thermochim. Acta*, 27 (1978) 45.
9 J. Suzuki and M. Ito, *J. Jpn. Assoc. Mineral. Petrol. Econ. Geol.*, 70 (1975) 79.
10 *Power Diffraction File*, Joint Committee on Powder Diffraction Standards, Swarthmore, U.S.A., 1977, Inorganic 8–179.
11 *Power Diffraction File*, Joint Committee on Powder Diffraction Standards, Swarthmore, U.S.A., 1977, Inorganic 20–669.
12 Y. Sawada, T. Ishiguro and M. Kato, *Seramikkusu*, 10 (1975) 163.
13 L. K. Frevel, *Ind. Eng. Chem.*, 14 (1942) 687.
14 L. K. Frevel, H. W. Rinn and H. C. Anderson, *Ind. Eng. Chem.*, 18 (1946) 83.
15 L. K. Frevel and H. W. Rinn, *Ind. Eng. Chem.*, 25 (1953) 1697.
16 J. C. Bell and A. E. Austin, *Battle Indexing Charts for Diffraction Patterns of Tetragonal, Hexagonal and Orthorhombic Crystals*, Battele Memorial Institute, Columbus, Ohio, U.S.A.
17 F. A. Miller and C. H. Wilkins, *Anal. Chem.*, 24 (1952) 1253.
18 G. Raade, *Am. Mineral.*, 55 (1970) 1457.
19 K. Nakamoto, *Kagaku No Ryoiki*, 14 (1963) 67.
20 W. B. White, *Am. Mineral.*, 56 (1971) 46.
21 I. Barin and O. Knacke, *Thermochemical Properties of Inorganic Substances*, Springer-Verlag, Heidelberg, 1973, pp. 163,441 and 450.